# **Experimental Analysis of Bubble Dynamics in The Presence of Fibers** in Aqueous Solution

Nurul Arifah Binti Ariffin<sup>1</sup>, Ryo Kurimoto<sup>1\*</sup>, Roberta Fátima Neumeister<sup>2</sup>, Gherhardt Ribatski<sup>2</sup>, Kosuke Hayashi<sup>1</sup>

- 1. Graduate School of Engineering, Kobe University, 1-1, Rokkodai, Nada, Kobe, 657-8501, Japan
- 2. Heat Transfer Research Group, São Carlos School of Engineering, University of São Paulo, 400 Trabalhador São-Carlense Ave, Parque Arnold Schimidt, São Carlos, SP 13566-590, Brazil \* Corresponding Author: kurimoto@mech.kobe-u.ac.jp

#### **Abstract**

The shapes and terminal velocities of single bubbles rising through a vertical fiber bundle in aqueous solutions were studied. The liquid phases were glycerol-water solutions and a xanthan-gum water solution which is a non-Newtonian fluid, in addition to water dealt with in our previous study. Fibers with 2 mm diameter were arranged in 4 x 4, 6 x 6 and 12 x 12 configurations, with pitches  $L_P$  of 18, 12 and 6 mm, respectively. The presence of fibers enhanced the terminal velocities with increasing number of fibers, i.e. decreasing  $L_P$ , regardless of liquid phases. This tendency was remarkable in the cap-bubble regime. Top view images indicated that the increase in velocity due to the presence of fibers would relate to the reduction in the projected area of bubbles. The drag coefficient correlation developed for bubbles in water was inadequate for those in the solutions of higher viscosities, requiring a revised model that implements the effect of viscosity.

# Keywords

Terminal velocity, Fiber bundle, Bubble shape, Projected area

## 1. Introduction

Membrane filtration is widely applied in water purification systems, e.g., hollow fiber membranes are used in membrane bioreactors (MBRs) to produce clean water by separating particulate contaminants from wastewater. In MBRs, aeration plays a key role not only in supplying oxygen to microbes, but also in preventing and removing deposits on the membrane surface. However, aeration consumes a large amount of energy, making it one of the major energy costs in MBR systems. It is therefore important to understand the behavior of bubbly flow inside and around bundles of hollow fiber membranes to develop more efficient aeration systems.

Our recent research [1] has focused on the shapes and terminal velocities of single bubbles rising through a fiber bundle in water, where the fibers of 2 mm in diameter were arranged in a square configuration. However, in actual MBRs, the viscosity of wastewater is much higher than that of water. In this study, the terminal velocity and shape of the single bubble rising in the fiber bundle were experimentally investigated with highly viscous aqueous solutions, that is, glycerol-water solutions and a xanthan gum-water solution, to understand the effects of liquid viscosity on the bubble dynamics.

## 2. Experimental Methods

Figure 1 shows the experimental setup, which consists of a square tank filled with a liquid phase and a fiber bundle secured within the tank. The fibers were 2 mm in diameter and made of transparent fluorinated ethylene propylene (FEP). A single bubble was released from the horizontal nozzle, which was placed 60 mm above the bottom of the bundle, by using gas syringe. The experiments were conducted under four conditions: no fibers and fiber bundles arranged in 4 x 4, 6 x 6 and 12 x 12 fiber configurations with the corresponding pitches  $L_P$  of 18, 12 and 6 mm, respectively. Glycerol water-solutions of 64 (GW64) and 74 wt% (GW74) as well as 0.8 g/L xanthan gum-water solution (XGW) were employed as the aqueous solutions. The viscosities of GW64 and GW74 were 13.18 and 27.94 mPa·s, respectively. Meanwhile for XGW, the viscosity ranged from 11.7 to 22.7 mPa·s and was

calculated based on Ostwald-de Waele relation. The rising motion of the bubbles was captured using a high-speed video camera and top view images were obtained using a borescope. The sphere-volume-equivalent bubble diameter d was calculated based on pre-determined volume based on the scale of the syringe, with values ranging from 4.2 mm to 19 mm.

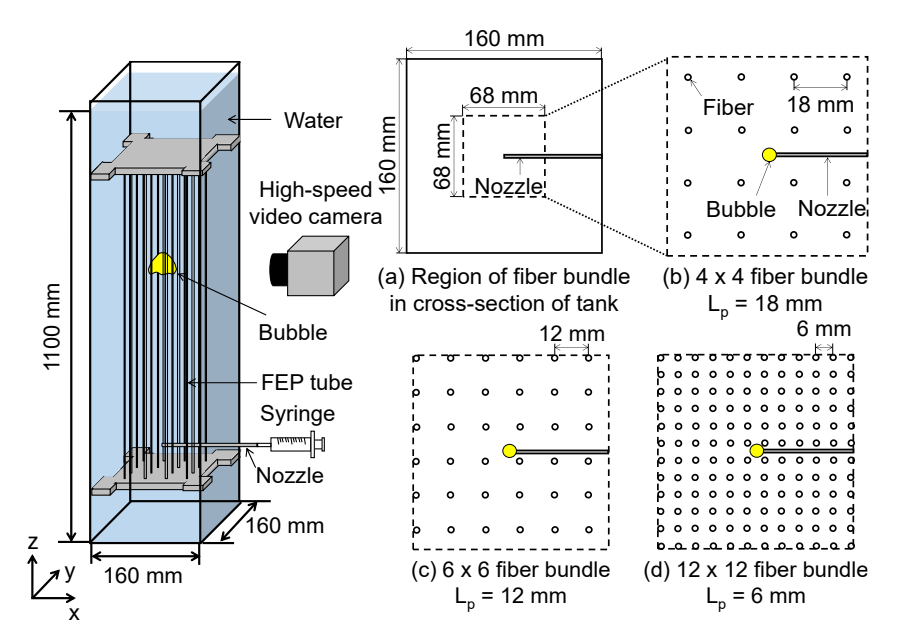


Figure 1 Experimental setup.

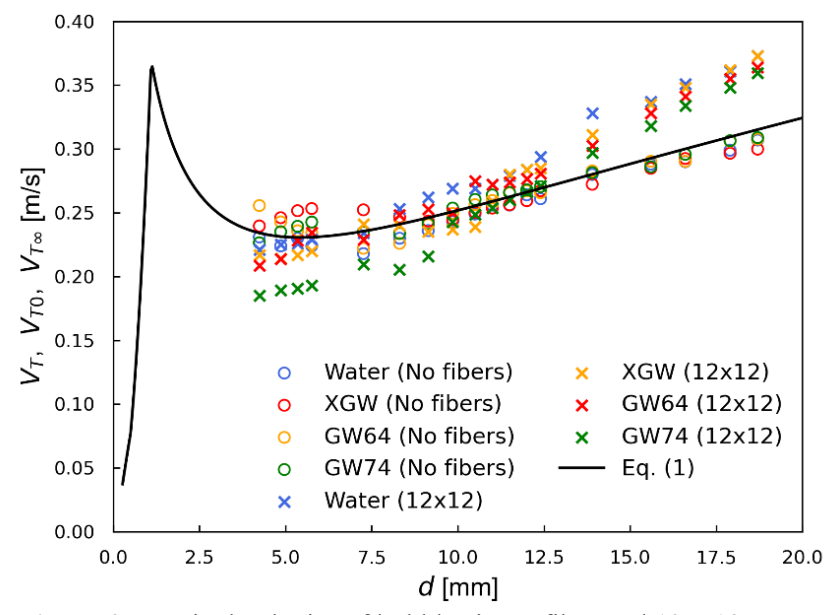
## 3. Results and Discussion

Figure 2 presents the terminal velocities,  $V_{T0}$ , for no fiber and those,  $V_T$ , for the 12 x 12 configuration in different aqueous solutions. For the no fiber case,  $V_{T0}$  in water and GW64 decrease as d increases up to 7.3 mm, and then increase for d > 7.3 mm. In contrast, for GW74 and XGW,  $V_{T0}$  increase with d up to 5.8 mm, then decrease until d = 8.3 mm and increase again for d > 8.3 mm. The bubbles of d = 5.8 mm exhibited transition from rectilinear to oscillation bubble path regime in GW74 and XGW. For d > 8.3 mm, the velocity trend in all aqueous solution align with the terminal velocity in an infinite stagnant liquid  $V_{T\infty}$ , which was calculated using the following drag [2]:

$$C_{D\infty} = \max \left\{ \min \left[ \frac{16}{Re_{\infty}} \left( 1 + 0.15 \, Re_{\infty}^{0.687} \right), \frac{48}{Re_{\infty}} \right], \frac{8}{3} \frac{Eo}{Eo + 4} \right\}$$
 (1)

where  $Re_{\infty}$  and Eo are the bubble Reynolds number in infinite stagnant liquids and the Eötvös number. Here, the physical properties of water were used for the calculation. The agreement with the no fiber case data suggests that for larger bubbles, the effect of viscosity on terminal velocity becomes negligible.

For the 12 x 12 configuration case,  $V_T$  tends to be faster than  $V_{T0}$  for  $d \ge 8.3$  mm in water and for  $d \ge 11.5$  mm in the aqueous solutions. This trend becomes remarkable in the cap bubble-regime, i.e., for  $d \ge 13.9$  mm. For all aqueous solutions, the no fiber case shows the slowest bubbles, followed by the 4 x 4, 6 x 6 and 12 x 12 configurations, i.e.,  $V_T$  increases as  $L_P$  decreases.



**Figure 2** Terminal velocity of bubbles in no fiber and 12 x 12 cases.

As the three-dimensional shape of bubbles could not be comprehended by horizontal images alone, a borescope was inserted from the top of the 12 x 12 configuration setup. Figure 3 shows the synchronized images of the side and top of a bubble with d=18.7 mm in GW74. The bubble interface observed from the top view is outlined with red line, revealing a cross-like shape. This shape deformation is consistently observed across all liquid phases, indicating that the liquid viscosity does not significantly influence the shape deformation. From this observation, bubbles in the 4 x 4, 6 x 6 and 12 x 12 configurations are expected to adopt a cross-like shape when d is larger than  $L_P$ .

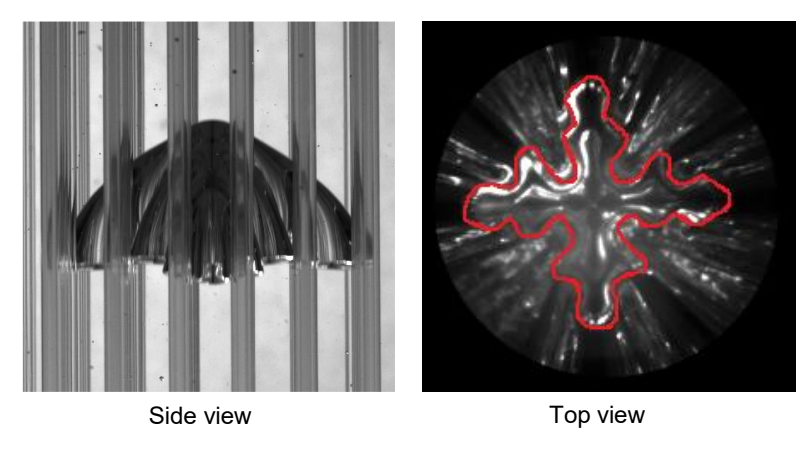


**Figure 3** Side and top views of bubbles in 12 x 12 configuration.

Figure 4 illustrates the relationship between d and the area ratio which is defined as the ratio of the actual projected area of a bubble to that in no fiber. For the 12 x 12 configuration case, the projected area was measured from the top view images whereas for the no fiber case, it was assumed to be circular, the diameter of which was obtained from the side view. The area ratio is smaller than unity across all diameters and exhibits a decreasing trend with increasing d. This clearly demonstrates that the presence of fibers causes the reduction in the bubble projected area and is particularly remarkable in cap-bubbles regime.

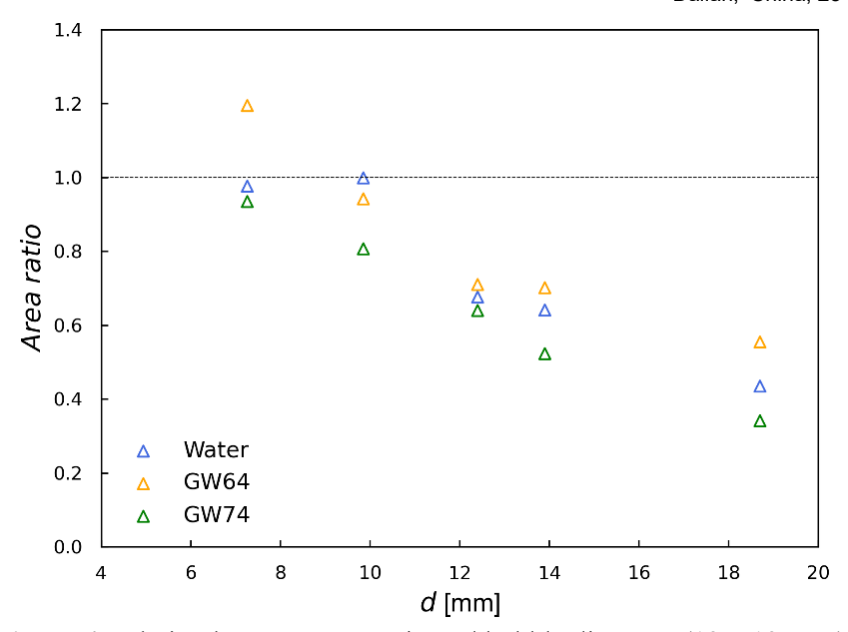


Figure 4 Relation between area ratio and bubble diameter (12 x 12 case).

Based on the balance between the drag and buoyant forces:

$$\frac{1}{2}C_{DA}\rho_L V_T^2 S = (\rho_L - \rho_G)gV \tag{2}$$

the increase in the terminal velocity is balanced by the corresponding reduction in the projected area S for the same d. Here,  $\rho_L$  and  $\rho_G$  are the densities of the liquid and gas phases, respectively, g is the gravitational acceleration, and V is the bubble volume. The drag coefficient,  $C_{DS}$ , resulting from using d for S was larger  $C_{DA}$  which was calculated based on actual projected area. Bubbles that exhibit a cross-like shape in the presence of fibers have higher  $C_{DA}$  than the circular shape in the no fiber case, whereas the reduction of S overcome that  $C_{DA}$  increase, resulting in the increase in  $V_T$ .

The drag coefficient correlation proposed in Ref.[1] is expressed as

$$C_{DS} = C_{DS} \Phi_W (1 + \Phi_f) \tag{3}$$

where  $\Phi_W$  and  $\Phi_f$  represent the wall and fiber effect multipliers, respectively. The  $\Phi_f$  is defined as the ratio of  $C_{DS}$  in the presence of fibers to that in its absence. Figure 5 shows the relation between  $\Phi_f$  and  $\lambda_f$ , where  $\lambda_f$  is defined as the ratio of d to  $L_P$  and the solid line is the following correlation for bubbles in water:

$$\Phi_f = -0.0773 \,\lambda_f^{1.29} \tag{4}$$

The data were selected for the Eötvös number corresponding to the bubbles that are dominantly influenced by the inertial force. The boundary between the surface tension and inertial force regimes varies with the Morton number and were therefore identified based on the velocity trends in the no fiber cases. The  $\Phi_f$  decreases as  $\lambda_f$  increases regardless of fiber arrangement. Although the decreasing trend of  $\Phi_f$  is observed in all cases as predicted by Eq. (4), most of the data do not fit well with the correlation, indicating the influence of viscous effect should be implemented in  $\Phi_f$ . In particular, for  $\lambda_f \ge 2$ , the shape deformation due to the presence of fibers does not depend much on viscosity. However, the observed deviation may result from interaction with fibers that involves the effect of viscosity.

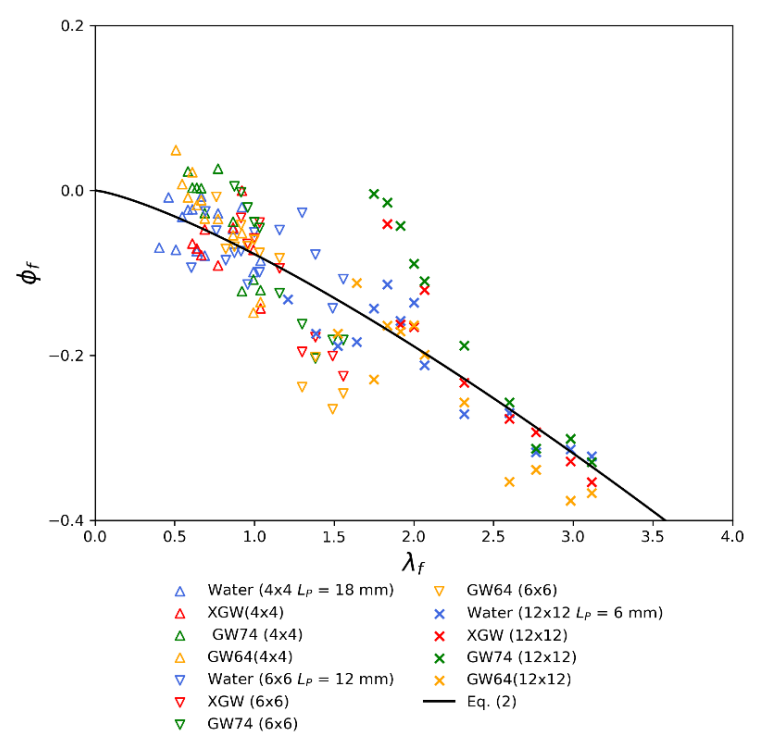


Figure 5 Relation between  $\Phi_f$  and  $\lambda_f$ .

#### 4. Conclusion

The presence of fibers increased the terminal velocities with increasing number of fibers, i.e. decreasing fiber pitches  $L_P$ . This tendency was remarkable in the cap-bubble regime. In this regime, top view images revealed that bubbles rising through a bundle of fibers exhibit a cross-like shape, resulting in a smaller projected area compared to that in the no fiber case. This deformation was consistently observed in all liquid phases. Based on the balance between drag and buoyant forces, the reduction in projected area resulted in the increase in terminal velocity. The correlation of drag coefficient developed for water case does not accurately evaluate the drag coefficients measured in the aqueous solutions. Therefore, a revised model that implements the viscous effect into the fiber effect multiplier is required.

## **Acknowledgements**

This publication was subsidized by JKA through its promotion funds from KEIRIN RACE (25MC1202-009). This research was also supported by JSPS KAKENHI (Grant No. 23K03660).

## Reference

- [1] Kurimoto, R., et al., Shapes and terminal velocities of single bubbles rising through fiber bundle in stagnant water, Chemical Engineering Science, 2024, 299:120557.
- [2] Tomiyama, A., et al., Drag coefficients of single bubbles under normal and micro gravity conditions, JSME International Journal Series B Fluids and Thermal Engineering, 1998, 41(2):472-479.